Formation of secondary aerosols from gasoline vehicle exhaust when mixing with SO_2

Tengyu Liu[1,2], Xinming Wang[1]*, Qihou Hu[1], Wei Deng[1,2], Yanli Zhang[1], Xiang Ding[1], Xiaoxin Fu[1,2], Fran ̧ois Bernard[1,3], Zhou Zhang[1,2], Sujun L ̈[1,2], Quanfu He[1,2], Xinhui Bi[1], Jianmin Chen[4], Yele Sun[5], Jianzhen Yu[6], Pingan, Peng[1], Guoying Sheng[1], Jiamo Fu[1]

1. State Key Laboratory of Organic Geochemistry, Guangzhou Institute of Geochemistry, Chinese Academy of Sciences, Guangzhou 510640, China.
2. University of Chinese Academy of Sciences, Beijing 100049, China.
3. Chemical Sciences Division, NOAA Earth System Research Laboratory, Boulder, Colorado 80305, USA.
4. Shanghai Key Laboratory of Atmospheric Particle Pollution and Prevention, Department of Environmental Science & Engineering, Fudan University, Shanghai 200433, China.
5. Institute of Atmospheric Physics, Chinese Academy of Sciences, Beijing 100029, China.
6. Division of Environment, Hong Kong University of Science & Technology, Clear Water Bay, Kowloon, Hong Kong, China.

*Corresponding author:

Dr. Xinming Wang

State Key Laboratory of Organic Geochemistry

Guangzhou Institute of Geochemistry, Chinese Academy of Sciences

23 Tel: +86-20-85290180; Fax: +86-20-85290706

24 Email: wangxm@gig.ac.cn

25

Abstract

Sulfur dioxide (SO_2) can enhance the formation of secondary aerosols from biogenic volatile organic compounds (VOCs), but its influence on secondary aerosol formation from anthropogenic VOCs, particularly complex mixtures like vehicle exhaust, remains uncertain. Gasoline vehicle exhaust (GVE) and SO_2, a typical pollutant from coal burning, are directly co-introduced into a smog chamber, in this study, to investigate the formation of secondary organic aerosols (SOA) and sulfate aerosols through photooxidation. New particle formation was enhanced while substantial sulfate was formed through the oxidation of SO_2 in the presence of high concentration of SO_2. Homogenous oxidation by OH radicals contributed a negligible fraction to the conversion of SO_2 to sulfate, and instead the oxidation by stabilized Criegee intermediates (sCIs), formed from alkenes in the exhaust reacting with ozone, dominated the conversion of SO_2. After 5 h of photochemical aging, GVE's SOA production factor revealed an increase by 60–200% in the presence of high concentration of SO_2. The increase could principally be attributed to acid-catalyzed SOA formation as evidenced by the strong positive linear correlation (R^2 = 0.97) between the SOA production factor and in-situ particle acidity calculated by AIM-II model. A high-resolution time-of-flight aerosol mass spectrometer (HR-TOF-AMS) resolved OA's relatively lower oxygen-to-carbon (O:C) (0.44±0.02) and higher hydrogen-to-carbon (H:C) (1.40±0.03) molar ratios for the GVE/SO_2 mixture, with a significantly lower estimated average carbon oxidation state (OS_c) of -0.51±0.06 than -0.19±0.08 for GVE alone. The relative higher mass loading of OA in the experiments

48 with SO_2 might be a significant explanation for the lower SOA oxidation degree.

1. Introduction

Sulfate and organic aerosols (OA) can lead to serious and complex air pollution (Parrish and Zhu, 2009) as the main components of fine particles or $PM_{2.5}$, conveying negative effects on human health (Nel, 2005). Sulfate and OA additionally affect radiative forcing on a global scale (Andreae et al., 2005; Shindell et al., 2009). Thus, a detailed understanding of the magnitude and formation pathways of sulfate and OA is critical to formulate control strategies and to accurately estimate their impact on air quality and climate. Complications often arise due to missing or underestimated oxidation pathways of sulfur dioxide (SO_2) (Berglen et al., 2004), the precursor of sulfate, and the unclear formation mechanisms of secondary organic aerosols (SOA) (de Gouw et al., 2005; Heald et al., 2005; Johnson et al., 2006; Volkamer et al., 2006), accounting for a large fraction of OA (Zhang et al., 2007).

Recent smog chamber studies have demonstrated that the amount of SOA formed from dilute gasoline vehicle exhaust often exceeds primary OA (POA) (Nordin et al., 2013; Platt et al., 2013; Gordon et al., 2014; Liu et al., 2015). Aromatic hydrocarbons were found to be vital SOA precursors in gasoline vehicle exhaust. Up to 90% of SOA from idling Euro 1–4 vehicle exhaust could be attributed to aromatics (Nordin et al., 2013; Liu et al., 2015). Gordon et al. (2014) concluded that traditional precursors could fully explain the SOA production from old vehicles with model years prior to 1995. Emitted primarily from coal-fired power plants and coal-burning boilers, SO_2, when mixed with gasoline vehicle exhaust containing the precursors for secondary nitrates and organic aerosols, NO_x and aromatics, may react, complicating the

formation of sulfate and SOA. Alkenes present in gasoline vehicle exhaust can react with ozone to form stabilized Criegee intermediates (sCIs), recently considered to significantly oxidize SO_2 and influence sulfate formation (Mauldin et al., 2012; Welz et al., 2012). On the other hand, recent smog chamber simulations indicated that SO_2 could enhance SOA formation from typical biogenic precursors, such as monoterpenes and isoprene through acid-catalyzed reactions (Edney et al., 2005; Kleindienst et al., 2006; Jaoui et al., 2008), but the influence of acid-catalyzed reactions on SOA formation from aromatics still remains debatable (Cao and Jang, 2007; Ng et al., 2007). Combinations of several pure chemicals, additionally, are not fully representative of SO_2 mixing with vehicle exhaust containing thousands of gaseous and particle-phase components (Gordon et al., 2014) in the formation of secondary aerosols under real atmospheric conditions. Till present no reports are available about the influence of SO_2 on secondary aerosol formation from complex vehicle exhaust.

Here we directly introduced pipe exhaust from light-duty gasoline vehicles (LDGV) and SO_2 into a smog chamber with a 30 m^3 Teflon reactor (Wang et al., 2014), to study the production of secondary aerosols: the influence of LDGV exhaust on SO_2 oxidation to form sulfate aerosols and reciprocally that of SO_2 on SOA formation from primary organics in LDGV exhaust.

2. Materials and methods

2.1 Vehicles and fuel

In Europe, vehicle emissions are classified by “Euro Standards”, currently ranging

from Euro 1 to Euro 6. China implemented the Euro 1, Euro 2, Euro 3 and Euro 4 emission standards in 2000, 2004, 2007 and 2012 for LDGVs and the Euro 5 standard will be implemented in 2018. Three LDGVs were utilized in this study, one Euro 1 and two Euro 4 vehicles. They are all port fuel injected vehicles with model years ranging from 2002 to 2011. Further vehicle details are listed in Table 1. All vehicles were fueled with Grade 93# gasoline, which complies with the Euro III gasoline fuel standard. Details of the gasoline composition can be found elsewhere (Zhang et al., 2013).

2.2 Smog chamber experiments

Six photochemical experiments with LDGV exhaust were conducted in a 30 m^3 indoor smog chamber at Guangzhou Institute of Geochemistry, Chinese Academy of Sciences (GIG-CAS). Details of the smog chamber were described by Wang et al. (2014). Briefly, black lamps (1.2m-long, 60W Philips/10R BL, Royal Dutch Philips Electronics Ltd, The Netherlands) are used as a light source, providing a NO_2 photolysis rate of 0.49 min^{-1}. Two Teflon-coated fans are installed inside the reactor to guarantee thorough mixing of the introduced gas species and particles within 120 seconds. Temperature and relative humidity in the reactor were controlled at approximately 25 ℃ and 50%, respectively. A schematic of the experiment setup is presented in Fig. 1. Eight thermocouples are placed between the enclosure and the reactor walls to control the temperature. The temperature inside the reactor (T9) was measured by Siemens QFM2160 (Siemens AG, Germany).Vehicles were first operated on-road to warm up the three-way catalysts for a minimal half an hour prior

115 to introducing the vehicle exhaust. Idling vehicle exhaust was then introduced directly
116 by two oil-free pumps (Gast Manufacturing, Inc, USA) into the reactor at a flow rate
117 of 40 L min^{-1}. Losses of volatile organic compounds (VOCs) and particles in the
118 transfer lines were estimated to be less than 5% (Liu et al., 2015). Prior to each
119 experiment, the chamber was evacuated and filled with purified dry air for at least 5
120 times, then the reactor was flushed with purified dry air for a minimal 48 h until no
121 residual hydrocarbons, O_3, NO_x, or particles were detected in the reactor. The exhaust
122 in the reactor was diluted by a factor of 13–94 compared to the tailpipe.

123 SO_2 was injected by a gas-tight syringe following introduction of exhaust to
124 create a mixing ratio of SO_2 in the reactor of approximately 150 ppb during three
125 experiments with the three vehicles. Experiments without additional SO_2 were also
126 conducted for each vehicle to compare and additional NO was added to adjust the
127 VOC/NO_x ratios (ppb/ppb) to between 4.9 and 10.8 (Table 2). VOC/NO_x ratios in
128 experiments with the same vehicle were similar with initial concentrations of NO_x
129 ranging from 300.8 to 458.5 ppb. After more than half an hour of primary
130 characterization, the exhaust was exposed to black light continuously for 5 h. The
131 formed SOA was characterized for another 2 to 3 h after the black lamps were
132 switched off to correct the particles wall loss. OH precursor and seed particles were
133 not introduced in this study.

134 An array of instruments was used to characterize gas and particle phase
135 compounds in the reactor. Gas phase NO_x, O_3 and SO_2 were measured with dedicated
136 monitors (EC9810, 9841T, Ecotech, Australia, and Thermo Scientific Model 43iTLE,

137 USA). The detection limit and accuracy of the SO_2 instrument are 0.2 ppb and ±1 %,
138 respectively. Methane and CO concentrations were determined using a gas
139 chromatography (Agilent 6980GC, USA) with a flame ionization detector and a
140 packed column (5A Molecular Sieve 60/80 mesh, 3 m × 1/8 inch) (Zhang et al., 2012).
141 CO_2 was analyzed with a HP 4890D gas chromatography (Yi et al., 2007). Gas phase
142 organic species were measured with a Mode 7100 preconcentrator (Entech
143 Instruments Inc., USA) coupled with an Agilent 5973N gas chromatography-mass
144 selective detector/flame ionization detector/electron capture detector (GC-MSD/FID,
145 Agilent Technologies, USA) (Wang and Wu, 2008, Zhang et al., 2010, 2012, 2013)
146 and a commercial proton-transfer-reaction time-of-flight mass spectrometer
147 (PTR-TOF-MS, Model 2000, Ionicon Analytik GmbH, Austria) (Lindinger et al.,
148 1998; Jordan et al., 2009). C_2-C_3 and C_4-C_{12} hydrocarbons were measured by GC-FID
149 and GC-MSD, respectively. PTR-TOF-MS was used to determine the time-resolved
150 concentrations of VOCs such as aromatics. The decay curve of toluene was used to
151 derive the average hydroxyl radical (OH) concentration during each experiment.

152 Particle number concentrations and size distributions were measured with a
153 scanning mobility particle sizer (SMPS, TSI Incorporated, USA, classifier model
154 3080, CPC model 3775). An aerosol density of 1.4 g cm^{-3} was assumed to convert the
155 particle volume concentration into the mass concentration (Zhang et al., 2005). A
156 high-resolution time-of-flight aerosol mass spectrometer (HR-TOF-MS, Aerodyne
157 Research Incorporated, USA) was used to measure the particle chemical compositions
158 and nonrefractory PM mass (Jayne et al., 2000; DeCarlo et al., 2006). The instrument

159 was operated in the high sensitivity V-mode and high resolution W-mode alternatively
160 every two minutes. The toolkit Squirrel 1.51H was used to obtain time series of
161 various mass components (sulfate, nitrate, ammonium and organics). We used the
162 toolkit Pika 1.1H to determine the average element ratios of organics, including H:C,
163 O:C, and N:C (Aiken et al., 2007, 2008). The contribution of gas-phase CO_2 to the
164 m/z 44 signal was corrected with measured CO_2 concentrations. The HR-TOF-MS
165 was calibrated using 300 nm monodisperse ammonium nitrate particles.

166 A summary of initial experimental conditions and final results is presented in
167 Table 2 and Table 3, respectively. Total wall-loss corrected OA varied from 17.8 to
168 91.4 μg m^{-3}, which spans the typical urban PM concentrations in heavy polluted
169 megacities with poor air quality. POA concentrations of the experiments ranged from
170 0.13 to 0.31 μg m^{-3} and are negligible compared with the formed SOA. Initial mixing
171 ratios of non-methane hydrocarbons (NMHCs) in the reactor were between 2.2 and
172 4.3 ppm, much higher than typical urban conditions. The average OH concentrations
173 during photo-oxidation ranged from 0.73 to 1.29×10^6 molecules cm^{-3}, approximately
174 5 times lower than that during summer daytime (Seinfeld and Pandis, 1998). Initial
175 concentrations of the reactants were maintained as similar as possible for the same
176 vehicle, though initial NMHCs, NO_x and average OH concentrations are different
177 from typical urban conditions, so all changes in SOA mass could be attributed to the
178 effects of SO_2.

179 **2.3 SOA production factors**

180 SOA production factor (PF) (mg kg^{-1}) is calculated on a fuel basis:

$$PF = 10^6 \cdot [SOA] \cdot \left(\frac{[\Delta CO_2]}{MW_{CO_2}} + \frac{[\Delta CO]}{MW_{CO}} + \frac{[\Delta HC]}{MW_{HC}}\right)^{-1} \cdot \frac{\omega_C}{MW_C} \quad (1)$$

where $[\Delta CO_2]$, $[\Delta CO]$, and $[\Delta HC]$ are the background corrected concentrations of CO_2, CO and the total hydrocarbons in the reactor in μg m^{-3}; [SOA] is the concentration of wall-loss corrected SOA in μg m^{-3}; MW_{CO2}, MW_{CO}, MW_{HC}, and MW_C are the molecular weights of CO_2, CO, HC and C. ω_C (0.85) is the carbon intensity of the gasoline (Kirchstetter et al., 1999). Total hydrocarbons measured in this study include methane and C_2-C_{12} hydrocarbons. The carbon content of each hydrocarbon was respectively calculated and then summed in Eq. (1).

2.4 Determination of OH concentration

Decay of toluene measured by PTR-TOF-MS is used to determine the average OH concentration during each experiment. Changes in the toluene concentration over time can be expressed as:

$$\frac{d[toluene]}{dt} = -k \cdot [OH] \cdot [toluene] \quad (2)$$

where k is the rate constant for the reaction between toluene and OH radical. The value of k is obtained from the Master Chemical Mechanism version 3.3 or MCM v3.3 (http://www.chem.leeds.ac.uk/MCM) (Jenkin et al., 2003). Assuming a constant OH concentration during an experiment, we can integrate Eq. (2) to get Eq. (3):

$$\ln\left(\frac{[toluene]_0}{[toluene]_t}\right) = k \cdot [OH] \cdot t \quad (3)$$

So by plotting $ln([\text{toluene}]_0/[\text{toluene}]_t)$ versus time t, we can obtain a slope that equals $k \times [OH]$. The average OH concentration is then calculated as:

$$[OH] = \frac{slope}{k} \quad (4)$$

Average OH concentrations were determined when the black lamps were on. Segmented OH concentrations were also estimated and listed in Table S1 in the Supplement for experiments with the addition of SO_2. Similar concentrations of sCIs were determined in subsequent section 2.5 when average and segmented OH concentrations were respectively used for the same experiment.

2.5 Determination of the steady state concentration of sCIs

Ozonolysis of alkenes will form a primary ozonide through a 1,3-cycloaddition of ozone across the olefinic bond. The primary ozonide then rapidly decomposes to two carbonyl compounds, called excited CIs, which can be stabilized by collision to form sCIs (Heard et al., 2004; Johnson and Marston, 2008).

$$\text{alkene} + O_3 \longrightarrow \phi\text{sCIs} + \text{products} \qquad \text{(R1)}$$

where ϕ represents the yield of sCIs from ozonolysis of alkenes. The four main losses of sCIs are reactions with H_2O, SO_2 and NO_2 and unimolecular decomposition.

$$\text{sCIs} + H_2O \longrightarrow \text{products} \qquad \text{(R2)}$$

$$\text{sCIs} + SO_2 \longrightarrow SO_3 + \text{products} \qquad \text{(R3)}$$

$$\text{sCIs} + NO_2 \longrightarrow \text{products} \qquad \text{(R4)}$$

$$\text{sCIs} \longrightarrow \text{products} \qquad \text{(R5)}$$

The steady state concentration of sCIs will be

$$[\text{sCIs}]_{\text{steady state}} = \frac{\phi K_{R1}[O_3][\text{alkene}]}{K_{R2}[H_2O] + K_{R3}[SO_2] + K_{R4}[NO_2] + K_{R5}} \qquad (5)$$

where K_{R1} is the rate coefficient for the ozonolysis of alkene; K_{R2}, K_{R3}, K_{R4} and K_{R5} represent the rate constant for reactions of sCIs with H_2O, SO_2, NO_2 and

223 decomposition, respectively. This equation was widely used to predict the steady state
224 concentration of sCIs in the atmosphere (Welz et al., 2012; Newland et al., 2015).

225 The steady state concentration of sCIs throughout the entire experiment was
226 estimated in this study. The production rate of sCIs was dependent on both the
227 concentrations and composition of alkenes in the exhaust. Detailed gas-phase
228 mechanisms of alkenes from the MCM v3.3 were run to determine the time-resolved
229 concentrations of sCIs in the experiments. The concentrations of alkenes included in
230 the model and the category of sCIs are presented in Table 4. N-alkenes and branched
231 alkenes respectively contributed 89.9%-93.0% and 7.0%-10.1% of the alkenes, with
232 ethene and propene as two main components accounting for 66.8%-81.3%. Only the
233 gas-phase mechanisms of alkenes were included in the model, with the concentrations
234 of OH radicals, SO_2, O_3 and NO_2 constrained to measured concentrations. Thus, the
235 neglect of alkanes and aromatics would not influence the steady state concentrations
236 of sCIs, as was confirmed by running the models including alkanes and aromatics.
237 K_{R2}, K_{R3}, K_{R4} and K_{R5} for CH_2OO, CH_3CHOO, and $(CH_3)_2COO$ used in the model
238 were listed in Table 5. The rate coefficients for other sCIs including C_2H_5CHOO,
239 C_3H_7CHOO, $C_2H_5(CH_3)COO$ and $(CH_3)_2CHCHOO$ reacted with H_2O, SO_2, NO_2 and
240 their unimolecular decomposition were assumed to be same as CH_2OO. This
241 assumption seems reasonable as the precursors of C_2H_5CHOO, C_3H_7CHOO,
242 $C_2H_5(CH_3)COO$ and $(CH_3)_2CHCHOO$ contributed only a small portion of alkenes in
243 this study. The yields of CH_2OO, CH_3CHOO, and $(CH_3)_2COO$ used in the model were

244 0.37, 0.38 and 0.28, respectively, while yields of other sCIs were assumed to be same
245 as CH_2OO.

246 **2.6 Wall loss corrections**

247 The loss of particles and organic vapors onto the reactor walls must be accounted for
248 to accurately quantify the SOA production. A detailed discussion of these corrections
249 can be found elsewhere (Liu et al., 2015). The loss of particles onto the walls was
250 treated as a first-order process (McMurry and Grosjean, 1985). The wall-loss rate
251 constant was determined separately for each experiment by fitting the SMPS and
252 AMS data with first-order kinetics when UV lamps were switched off. By applying
253 this rate to the entire experiment, we use the same method as Pathak et al. (2007) to
254 correct the wall loss of the particles. The wall loss of particles is a size-dependent
255 process, therefore, the presence of nucleation would influence wall loss correction of
256 the particles due to the rapid loss of nucleation mode particles. As shown in a previous
257 study, particle wall loss rates could not be accurately quantified for the particles
258 generated in the nucleation event (Keywood et al., 2004). The impact of the
259 nucleation event on wall-loss estimate is considered to be negligible as less than 5%
260 of the particle mass is in the nucleation mode twenty minutes after nucleation for all
261 experiments in this study.

262 Wall deposition of organic vapors can lead to the underestimation of SOA
263 production (Matsunaga and Ziemann, 2010; X. Zhang et al., 2014, 2015). Wall
264 deposition of a compound has recently been established as related with its volatility
265 (Zhang et al., 2015). The extent that wall deposition of organic vapors impacts on

SOA production depends on the competition of organic vapors depositing onto walls and suspended particles. Here, we assumed that gas-particle partitioning of organic vapors dominated their wall depositions and thus organic vapors were considered to only partition onto suspended particles.

As the collection efficiency of sulfate in the HR-TOF-AMS can vary due to the coating of OA onto sulfate, we used AMS data combined with SMPS data to derive the time-resolved concentrations of OA, sulfate, ammonium and nitrate. The emission of black carbon (BC) from LDGVs was negligible according to a previous study (Liu et al., 2015), thus the ratio of OA to inorganic aerosols from the AMS was used to split the total particle mass measured by SMPS into the mass of OA, sulfate, ammonium and nitrate (Gordon et al., 2014; Liu et al., 2015).

3. Results and discussion

3.1 Formation of sulfate

Fig. 2 shows the temporal evolution of gas– and particle–phase species during the photochemical aging of emissions from vehicle III with and without adding SO_2. NO was injected to adjust the VOC/NO_x ratio at approximately time = -0.25 h for both experiments. After the black lamps were switched on, NO was rapidly consumed in less than 1 h. Mass concentrations of secondary aerosols rapidly ascended following photooxidation with or without SO_2 for approximately 1 h, stabilizing after approximately 4 h of photo-oxidation (Figs. 2, 3, and 4). Substantial sulfate was formed synchronously with OA for experiments with SO_2 with the maximum particle number concentrations at 5.4–48 times of those without SO_2 (Table 1, Fig. 5),

indicating enhanced new particle formation (NPF) when adding SO_2. As the precursor of sulfuric acid (H_2SO_4), SO_2 at higher concentrations would lead to additional formation of H_2SO_4, thereby increasing the nucleation rates and total particle number concentrations (Sipila et al., 2010). The S-bearing organic fragments $C_xH_yO_zS$ determined by HR-TOF-AMS can be used as marker ions to quantify organosulfates (Huang et al., 2015). In this study the fragments $C_xH_yO_zS$ were almost not appreciable. Using the methods of Huang et al. (2015), we estimated the mass ratio of organosulfates to sulfate was less than 0.5%. Thus the formation of organosulfates could be negligible in this study.

Substantial nitrates were formed for vehicles I and II (Figs. 3a and 4a) and could be attributed to ammonium or organic nitrates. The identification of ammonium and organic nitrates may be obtained from the NO^+/NO_2^+ ratio, which is typically substantially higher for organic nitrates compared with ammonium nitrate (Farmer et al., 2010; Sato et al., 2010). The NO^+/NO_2^+ ratios for experiments I-2 and II-2 were 1.99-2.60, within the range 1.08-2.81 for ammonium nitrate (Farmer et al., 2010; Sato et al., 2010), suggesting that nitrates detected in the two experiments could be attributed to ammonium nitrate. Ammonium nitrate was likely formed by reactions of nitric acid formed from NO_x oxidation and ammonia, which is substantially higher in China's LDGV exhaust (Liu et al., 2014). The NO^+/NO_2^+ ratios for experiments with SO_2 were 3.9-5.0, significantly higher than ratios measured for ammonium nitrate and also similar to ratios for organic nitrates (3.82-5.84) from the photo-oxidation of aromatic hydrocarbons (Sato et al., 2010), indicating organic nitrates dominated

310 nitrate formation in these experiments. High concentration of SO_2 suppressed the
311 formation of ammonium nitrate in experiments with SO_2 as NH_3 was liable to react
312 with sulfuric acid rather than nitric acid (Pathak et al., 2009).

313 Formation rates of sulfate, derived from the differential of concentration-time
314 plots of sulfate, exhibited burst increases at the initial stage of sulfate formation and
315 then decreased to near zero 5 h after sulfate formation initiated (Fig. 6a). The
316 maximum formation rate of sulfate in experiments I–2, II–2 and III–2 was 61.5, 21.6
317 and 113 μg m^{-3} h^{-1}, respectively, extremely higher than the rate of 0.17–0.37 ppbv h^{-1}
318 (0.73–1.59 μg m^{-3} h^{-1} under NTP condition) through gas-phase oxidation of SO_2
319 during the daytime in the Pearl River Delta (PRD) region of China in the summer of
320 2006 (Xiao et al., 2009), and also more than ten times higher than the maximum
321 sulfate formation rate of 4.79 μg m^{-3} h^{-1} observed at an urban site in Beijing during
322 the Beijing Olympic Games in 2008 (Zhang et al., 2011). The formation rate of sulfate
323 was related to the concentrations of SO_2 and OH, which were respectively
324 approximately 7 times higher and 2-16 times lower than those in the study of Xiao et
325 al. (2009). Significant differences of sulfate formation rates between chamber and
326 ambient observations could, however, indicate that there might be other processes
327 dominating the oxidation of SO_2 rather than gas-phase oxidation by OH in this study.

328 SO_2 was typically deemed to be oxidized by OH radicals through homogeneous
329 reactions in gas-phase (Calvert et al., 1978), or by H_2O_2 and O_3 through in-cloud
330 processes in aqueous-phase (Lelieveld and Heintzenberg, 1992) that, however, could
331 be negligible in this study due to RH of approximate 50%. As shown in Fig. 7, the

loss rate of SO_2 through homogeneous reactions with OH radicals in the three experiments ranged from 0.0023 to 0.0034 h^{-1}, accounting for only 2.4%–4.6% of the total loss rate of SO_2. The initial concentrations of alkenes in the experiments with SO_2 varied from 248 to 547 ppb, contributing 7.7%–23.5% of the total NMHCs. The high content of alkenes in the exhaust might form a mass of sCIs through the reaction with ozone. Recent studies indicated the rate coefficient of CH_2OO with SO_2 was 50 to 10000 times larger than that used in tropospheric models (Welz et al., 2012). The oxidation of SO_2 by sCIs may be as significant as that by OH radicals in the atmosphere. The oxidation rate of SO_2 for experiments I-2 and III-2, through the reactions with sCIs, was calculated to be 0.065 ± 0.029 h^{-1} and 0.042 ± 0.020 h^{-1} (Fig. 7), respectively, accounting for 66.9% and 61.4% of the total loss rate of SO_2. Considering the variability of sCIs throughout the entire experiment, we concluded that sCIs were virtually responsible for the oxidation of SO_2 in experiments I-2 and III-2. The oxidation rate of SO_2 through the reactions with sCIs for the experiment II-2 was estimated to be 0.028 ± 0.015 h^{-1}, contributing 31.5% of the total loss rate of SO_2. The unexplained loss of SO_2 might be a result of heterogeneous oxidation in the presence of LDGV exhaust containing massive aerosols and gaseous species. He et al. (2014) found that SO_2 could react with NO_2 on the surface of mineral dust to promote the conversion of SO_2 to sulfate. As shown in Fig. 5, the initial particle number for vehicle II was approximately 5000 cm^{-3}, nearly 40-50 times higher than those for vehicle I and III, providing larger aerosol surface areas for the oxidation of SO_2 by NO_2. However, quantification of SO_2 oxidation by NO_2 on the surface of existing

aerosols is difficult due to the lack of reaction rate constant (He et al., 2014). We speculate that the reaction between SO_2 and NO_2 on the surface of existing aerosols might explain the difference between the total loss rate of SO_2 and the sum of sCIs and OH oxidation for vehicle II.

3.2 SOA production

Fuel-based SOA production factors (PF), expressed as SOA production in milligram (mg) after 5 h photooxidation of LDGV exhaust emitted when per kilogram (kg) gasoline was burned, all increased substantially when adding SO_2, 60%–200% above that without SO_2 (Fig. 8a), although the selected cars' emission standards varied from Euro-I to Euro-IV. The in-situ particle acidities at the time when SOA formation rate peaks were calculated as H^+ concentrations based on AIM-II model H^+–NH_4^+–SO_4^{2-}–NO_3^-–H_2O with gas-aerosol partitioning disabled (http://www.aim.env.uea.ac.uk/aim/model2/model2a.php) (Clegg et al., 1998; Wexler and Clegg, 2002). Inputs to the model include temperature, RH, [SO_4^{2-}], [NO_3^-], [NH_4^+] and [H^+]$_{total}$, calculated based on ion balance. SO_4^{2-}, NH_4^+ and NO_3^- contributed virtually all of the aerosol phase ions mass in this study, thus determining the aerosol acidity. Though other ions (i.e., Ca^{2+}, Mg^{2+}, K^+ and Na^+) had negligible influence on the aerosol acidity, it is worth noting that the reported values of H^+ may be the upper bound. The in-situ particle acidities with the addition of SO_2 were 1.6–3.7 times as high as those without the addition of SO_2 (Table 3). This elevated particle acidity could largely explain the higher PFs of SOA from LDGV exhaust with SO_2, supported by the strong positive linear correlations (R^2 = 0.965, P<0.01) between

SOA PFs and the in-situ particle acidities (Fig. 8b). Aromatic hydrocarbons are vital SOA precursors in gasoline vehicle exhaust (Nordin et al., 2013; Gordon et al., 2014; Liu et al., 2015). The influence of particle acidity on SOA formation from aromatics is still debatable. Cao and Jang (2007) found that the presence of acid seeds with [H^+] concentrations of 240-860 nmol m^{-3} significantly increased the SOA yields from oxidation of toluene and 1,3,5-trimethylbenzene compared with yields using neutral seed aerosols. However, Ng et al. (2007) observed no influence of particle acidity on SOA yields from the aromatics possibly due to the low content of aerosol water. SOA production from gasoline vehicle exhaust was enhanced in this study, even at a low level of [H^+] concentrations ranging from 7.4 to 27.1 nmol m^{-3}. Gas-phase oxidation products of aromatic hydrocarbons in the exhaust, like multifunctional carbonyl glyoxal, would be transformed more rapidly to low volatility products through acid-catalyzed heterogeneous reactions (Jang et al., 2002; Cao and Jang, 2007) and thus caused increasing SOA production. Aerosol water is needed for the hydration of carbonyls and therefore it influences the acid-catalyzed reactions. Liquid water content (LWC) in this study was not measured but predicted by the AIM-II model, with an average value of 5.5±4.5 μg m^{-3} when SOA formation rate peaks, ensuring the occurrence of acid-catalyzed reactions. Fig. 9 shows the ion intensity of fragment m/z 88 that can arise only from a glyoxal oligomer (Liggio et al., 2015). The scatter of the data might be due to the low intensity of m/z 88. However, the experiment with the addition of SO_2, with higher particle acidity, exhibited relatively higher m/z 88 intensity. This indicated the important role of acid-catalyzed heterogeneous reactions

in SOA formation from gasoline vehicle exhaust. A photo-oxidation experiment of exhaust from vehicle I in the presence of ammonium sulfate seeds (53.3 μg m^{-3}) with RH of 59% (Table 2) was conducted to explore the effect of sulfate on SOA formation as particle acidity is typically driven by sulfate. The SOA production factor was 22.2 mg kg^{-1} fuel, comparable with 26.2 mg kg^{-1} fuel for experiment I-1, indicating that sulfate may not directly influence SOA production. Thus, the SOA production was indeed dependent on the particle acidity.

The addition of SO_2 may vary the vapor wall loss rate and influence the estimation of SOA production. The wall accommodation coefficient ($\alpha_{w,i}$), governing the extent of wall deposition of a compound i, was observed to be inversely dependent on its effective saturation concentration C_i^* (X. Zhang et al., 2015). Partitioning coefficients for different C_i^* ranging from 0.01 to 10^6 μg m^{-3} were calculated using gas-particle partitioning theory (Donahue et al., 2006) (Table 6). Partitioning coefficients for experiments with and without the addition of SO_2 mainly exhibited big differences for C_i^* bins of 10 and 100 μg m^{-3} with $\alpha_{w,i}$ calculated to be 3.1×10^{-7} and 2.0×10^{-7}, respectively. The wall loss rate for C_i^* bin of 10 μg m^{-3} would then be approximately 50% higher than that for C_i^* bin of 100 μg m^{-3} assuming a linear relation between wall loss rate and $\alpha_{w,i}$ (X. Zhang et al., 2015). An increase of 50% in wall loss rate would lead to 11.5% higher vapor loss to walls when assuming the wall loss rate to be 2.0×10^{-5} s^{-1}, similar to a product of the photo-oxidation of toluene. Thus, biases of vapor wall loss rates due to the addition of SO_2 may have negligible influence on estimation of SOA production. Recent studies indicated that the presence

of high concentrations of seed aerosols might decrease the loss of organic vapors to the walls and thus increase the SOA formation (Kroll et al., 2007; X. Zhang et al., 2014, 2015). However, comparable SOA PFs for experiments with and without seed aerosols observed in this study indicated the negligible impact of seed aerosols on SOA production. Cocker III et al. (2001) also observed that the presence of ammonium sulfate seed aerosols had no impact on SOA formation from the photo-oxidation of m-xylene and 1,3,5-trimethylbenzene .

SOA formation rates, derived from the differential of concentration-time plots of SOA, exhibited similar trends as sulfate with a burst increase at the initial stage of SOA formation (Fig. 6b). The average SOA formation rates for vehicles I, II and III with SO_2 were 1.1, 1.2 and 4.4 times as high as those without SO_2, respectively, although the maximum rate for vehicle II with SO_2 was lower. Here we particularly focused on the burst increase stage of SOA and sulfate, which may be related to fast increase of $PM_{2.5}$ and occurrence of haze (He et al., 2014). Fig. 10 shows the correlation between SOA formation rate and particle acidity. Plotted data corresponded to data selected from Fig. 6 when SOA formation rate was higher than zero to when the rate reached the maximum value. Significant linear correlations ($P<0.05$, $R^2>0.88$) between SOA formation rate and particle acidity during this stage for experiments with SO_2 suggest that acid-catalyzed heterogeneous reactions might play an important role in the rapid formation of SOA (Jang et al., 2002). The fitted slopes for vehicle I, II and III were 3.96, 0.82 and 3.14, respectively, suggesting other factors, including alkene abundance, may influence the SOA formation rate. The

initial concentration of alkenes for experiments I-2, II-2 and III-2 was 547 ppb, 248 ppb and 353 ppb, respectively, consistent with the variation of the slopes. Higher alkene content would increase the formation rate of sCIs, which could rapidly oxidize SO_2 to sulfuric acid, thus influence the aerosol acidity.

3.3 Oxidation state

After 5 h of photo-oxidation, SOA's molar ratios of oxygen-to-carbon (O:C) and hydrogen-to-carbon (H:C) resolved by HR-TOF-AMS, were plotted on a Van Krevelen diagram (Heald et al., 2010) in Fig. 11. Concentrations of POA were lower than 0.5 μg m^{-3}, typically regarded as not appreciable (Presto et al., 2014) and insufficient to determine the initial H:C and O:C, thus only SOA data were plotted on the diagram. Relatively lower O:C (0.44±0.02) and higher H:C (1.40±0.03) for the mixture of SO_2 and exhaust were observed than those for exhaust alone. The oxidation state of carbon (OS_c), estimated from O:C and H:C, can be used to describe the chemistry and oxidative evolution of atmospheric organic aerosols (Kroll et al., 2011). Further calculated OS_c revealed an average lower level of -0.51±0.06 for SOA formed from LDGV exhaust with SO_2 when compared to that of -0.19±0.08 without SO_2, with all within or near the OS_c range of -0.5–0 for semi-volatile OOA (SV-OOA) (Aiken et al., 2008). The relatively lower OS_c with SO_2 indicated a lower oxidation degree of SOA. A difference in H:C and O:C for m-xylene SOA with neutral and acidic seed particles was not observed by Loza et al. (2012), thus acid-catalyzed heterogeneous reactions may not influence the oxidation degree of SOA in this study. Shilling et al. (2009) observed a lower O:C of SOA formed from the dark ozonolysis

of α-pinene at a higher mass loading of organic aerosols and suggested that compounds partitioning into the particle phase at lower loadings were more oxygenated. Kang et al. (2011) also observed that the oxidation degree of OA decreased rapidly as the OA mass concentration increased for the same amount of OH exposure. Given that the average OH concentrations were similar for the same vehicle (Table 2), the relative higher mass loading of OA in the experiments with SO_2 may lead to the lower O:C and thus decrease the oxidation degree of OA. The O:C ratios were observed to decrease 0.1 with an increase of approximately 50 μg m^{-3} of OA concentrations for m-xylene and p-xylene (Kang et al., 2011). However, in this study the slope was 0.1 ΔO:C for approximately 26 μg m^{-3} ΔOA. The differences may be due to that some other precursors other than aromatics contributed to SOA formation from gasoline vehicle exhaust (Liu et al., 2015).

The slope of -0.87 (Fig. 11) for the mixture of SO_2 and exhaust, slightly higher than those for exhaust alone (Liu et al., 2015), indicates that SOA formation in these experiments is a combination of carboxylic acid and alcohol/peroxide formation (Heald et al., 2010; Ng et al., 2011). The slope of -0.87 and intercept of approximately 1.8 are similar to the observation for ambient data with a slope of approximately -1 and intercept approximately 1.8 (Heald et al., 2010), suggesting that SOA chemistry for the mixture of SO_2 and gasoline vehicle exhaust is atmospheric relevant.

4. Conclusions

A series of chamber experiments investigating the formation of secondary aerosols from the mixture of SO_2 and gasoline vehicle exhaust were conducted. The high

content of alkenes in gasoline vehicle exhaust formed numerous sCIs, dominating the formation of sulfate while elevated particle acidity, resulting from the formation of sulfuric acid, enhanced SOA production from the gasoline vehicle exhaust. We concluded that SO_2 and gasoline vehicle exhaust can enhance each other in forming secondary aerosols. High concentration of SO_2 and high levels of aerosol acidity combined with rapid increase of LDGVs in heavily polluted cities such as Beijing (Pathak et al., 2009; He et al., 2014) might consequently worsen the air quality in the absence of stricter control strategies on emissions of SO_2 and vehicle exhaust. Previous studies indicated that high content of alkenes in China's gasoline oil was damaging for the control of ozone in ambient air (Y. Zhang et al., 2013, 2015). Our results suggested that the incomplete combustion of gasoline with high content of alkenes might also induce the formation of sCIs, facilitating the production of secondary aerosols. The limit of alkenes content in China was lowered to 24% by volume in the newly established Level V gasoline fuel standard from 28% by volume in the Level IV gasoline fuel standard. This limit remains substantially higher when compared to those in USA or in Europe, and in particular, 6 times that in California, USA. Thus, limiting the content of alkenes in China's gasoline might benefit the control of both ozone and secondary aerosols.

Acknowledgments

This study was supported by Strategic Priority Research Program of the Chinese Academy of Sciences (Grant No. XDB05010200), the Ministry of Science and

Technology of China (Project No. 2012IM030700), National Natural Science Foundation of China (Project No. 41025012/41121063) and Guangzhou Institute of Geochemistry (GIGCAS 135 project Y234161001).

513 **References**

514 Aiken, A. C., DeCarlo, P. F., and Jimenez, J. L.: Elemental Analysis of Organic
515 Species with Electron Ionization High-Resolution Mass Spectrometry, Analy.
516 Chem., 79, 8350-8358, doi:10.1021/ac071150w, 2007.

517 Aiken, A. C., DeCarlo, P. F., Kroll, J. H., Worsnop, D. R., Huffman, J. A., Docherty, K.
518 S., Ulbrich, I. M., Mohr, C., Kimmel, J. R., Sueper, D., Sun, Y., Zhang, Q.,
519 Trimborn, A., Northway, M., Ziemann, P. J., Canagaratna, M. R., Onasch, T. B.,
520 Alfarra, M. R., Prevot, A. S. H., Dommen, J., Duplissy, J., Metzger, A.,
521 Baltensperger, U., and Jimenez, J. L.: O/C and OM/OC Ratios of Primary,
522 Secondary, and Ambient Organic Aerosols with High-Resolution Time-of-Flight
523 Aerosol Mass Spectrometry, Environ. Sci. Technol., 42, 4478-4485,
524 doi:10.1021/es703009q, 2008.

525 Andreae, M. O., Jones, C. D., and Cox, P. M.: Strong present-day aerosol cooling
526 implies a hot future, Nature, 435, 1187-1190, 2005.

527 Berglen, T. F., Berntsen, T. K., Isaksen, I. S. A., and Sundet, J. K.: A global model of
528 the coupled sulfur/oxidant chemistry in the troposphere: The sulfur cycle, J.
529 Geophys. Res.-Atmos., 109, D19310, doi:10.1029/2003JD003948, 2004.

530 Calvert, J. G., Su, F., Bottenheim, J. W., and Strausz, O. P.: Mechanism of the
531 homogeneous oxidation of sulfur dioxide in the troposphere, Atmos. Environ., 12,
532 197-226, doi:10.1016/0004-6981(78)90201-9, 1978.

533 Cao, G., and Jang, M.: Effects of particle acidity and UV light on secondary organic
534 aerosol formation from oxidation of aromatics in the absence of NO_x, Atmos.

Environ., 41, 7603-7613, doi:10.1016/j.atmosenv.2007.05.034, 2007.

Clegg, S. L., Brimblecombe, P., and Wexler, A. S.: Thermodynamic Model of the System H^+−NH_4^+−SO_4^{2-}−NO_3^-−H_2O at Tropospheric Temperatures, J. Phys. Chem. A, 102, 2137-2154, doi:10.1021/jp973042r, 1998.

Cocker III, D. R., Mader, B. T., Kalberer, M., Flagan, R. C., and Seinfeld, J. H.: The effect of water on gas–particle partitioning of secondary organic aerosol: II. m-xylene and 1,3,5-trimethylbenzene photooxidation systems, Atmos. Environ., 35, 6073-6085, doi:10.1016/S1352-2310(01)00405-8, 2001.

de Gouw, J. A., Middlebrook, A. M., Warneke, C., Goldan, P. D., Kuster, W. C., Roberts, J. M., Fehsenfeld, F. C., Worsnop, D. R., Canagaratna, M. R., Pszenny, A. A. P., Keene, W. C., Marchewka, M., Bertman, S. B., and Bates, T. S.: Budget of organic carbon in a polluted atmosphere: Results from the New England Air Quality Study in 2002, J. Geophys. Res.-Atmos., 110, D16305, doi:10.1029/2004JD005623, 2005.

DeCarlo, P. F., Kimmel, J. R., Trimborn, A., Northway, M. J., Jayne, J. T., Aiken, A. C., Gonin, M., Fuhrer, K., Horvath, T., Docherty, K. S., Worsnop, D. R., and Jimenez, J. L.: Field-Deployable, High-Resolution, Time-of-Flight Aerosol Mass Spectrometer, Anal. Chem., 78, 8281-8289, doi:10.1021/ac061249n, 2006.

Donahue, N. M., Robinson, A. L., Stanier, C. O., and Pandis, S. N.: Coupled Partitioning, Dilution, and Chemical Aging of Semivolatile Organics, Environ. Sci. Technol., 40, 2635-2643, doi:10.1021/es052297c, 2006.

Edney, E. O., Kleindienst, T. E., Jaoui, M., Lewandowski, M., Offenberg, J. H., Wang,

W., and Claeys, M.: Formation of 2-methyl tetrols and 2-methylglyceric acid in secondary organic aerosol from laboratory irradiated isoprene/NO_x/SO_2/air mixtures and their detection in ambient $PM_{2.5}$ samples collected in the eastern United States, Atmos. Environ., 39, 5281-5289, doi:10.1016/j.atmosenv.2005.05.031, 2005.

Farmer, D. K., Matsunaga, A., Docherty, K. S., Surratt, J. D., Seinfeld, J. H., Ziemann, P. J., and Jimenez, J. L.: Response of an aerosol mass spectrometer to organonitrates and organosulfates and implications for atmospheric chemistry, P. Natl. Acad. Sci., 107, 6670-6675, doi:10.1073/pnas.0912340107, 2010.

Fenske, J. D., Hasson, A. S., Ho, A. W., and Paulson, S. E.: Measurement of Absolute Unimolecular and Bimolecular Rate Constants for CH_3CHOO Generated by the trans-2-Butene Reaction with Ozone in the Gas Phase, J. Phys. Chem. A, 104, 9921-9932, doi:10.1021/jp0016636, 2000.

Gordon, T. D., Presto, A. A., May, A. A., Nguyen, N. T., Lipsky, E. M., Donahue, N. M., Gutierrez, A., Zhang, M., Maddox, C., Rieger, P., Chattopadhyay, S., Maldonado, H., Maricq, M. M., and Robinson, A. L.: Secondary organic aerosol formation exceeds primary particulate matter emissions for light-duty gasoline vehicles, Atmos. Chem. Phys., 14, 4661-4678, doi:10.5194/acp-14-4661-2014, 2014.

He, H., Wang, Y., Ma, Q., Ma, J., Chu, B., Ji, D., Tang, G., Liu, C., Zhang, H., and Hao, J.: Mineral dust and NO_x promote the conversion of SO_2 to sulfate in heavy pollution days, Sci. Rep., 4, 4172, doi:10.1038/srep04172, 2014.

579 Heald, C. L., Jacob, D. J., Park, R. J., Russell, L. M., Huebert, B. J., Seinfeld, J. H.,
580 Liao, H., and Weber, R. J.: A large organic aerosol source in the free troposphere
581 missing from current models, Geophys. Res. Lett., 32, L18809,
582 do:10.1029/2005GL023831, 2005.
583 Heald, C. L., Kroll, J. H., Jimenez, J. L., Docherty, K. S., DeCarlo, P. F., Aiken, A. C.,
584 Chen, Q., Martin, S. T., Farmer, D. K., and Artaxo, P.: A simplified description of
585 the evolution of organic aerosol composition in the atmosphere, Geophys. Res.
586 Lett., 37, L08803, doi:10.1029/2010gl042737, 2010.
587 Heard, D. E., Carpenter, L. J., Creasey, D. J., Hopkins, J. R., Lee, J. D., Lewis, A. C.,
588 Pilling, M. J., Seakins, P. W., Carslaw, N., and Emmerson, K. M.: High levels of the
589 hydroxyl radical in the winter urban troposphere, Geophys. Res. Lett., 31, L18112,
590 doi:10.1029/2004GL020544, 2004.
591 Huang, D. D., Li, Y. J., Lee, B. P., and Chan, C. K.: Analysis of Organic Sulfur
592 Compounds in Atmospheric Aerosols at the HKUST Supersite in Hong Kong Using
593 HR-ToF-AMS, Environ. Sci. Technol., 49, 3672-3679, doi:10.1021/es5056269,
594 2015.
595 Jang, M., Czoschke, N. M., Lee, S., and Kamens, R. M.: Heterogeneous Atmospheric
596 Aerosol Production by Acid-Catalyzed Particle-Phase Reactions, Science, 298,
597 814-817, doi:10.1126/science.1075798, 2002.
598 Jaoui, M., Edney, E. O., Kleindienst, T. E., Lewandowski, M., Offenberg, J. H.,
599 Surratt, J. D., and Seinfeld, J. H.: Formation of secondary organic aerosol from
600 irradiated α-pinene/toluene/NO_x mixtures and the effect of isoprene and sulfur

601 dioxide, J. Geophys. Res. -Atmos., 113, D09303, doi:10.1029/2007JD009426,
602 2008.
603 Jayne, J. T., Leard, D. C., Zhang, X., Davidovits, P., Smith, K. A., Kolb, C. E., and
604 Worsnop, D. R.: Development of an Aerosol Mass Spectrometer for Size and
605 Composition Analysis of Submicron Particles, Aerosol. Sci. Tech., 33, 49-70,
606 doi:10.1080/027868200410840, 2000.
607 Jenkin, M. E., Saunders, S. M., Wagner, V., and Pilling, M. J.: Protocol for the
608 development of the Master Chemical Mechanism, MCM v3 (Part B): tropospheric
609 degradation of aromatic volatile organic compounds, Atmos. Chem. Phys., 3,
610 181-193, doi:10.5194/acp-3-181-2003, 2003.
611 Johnson, D., Utembe, S. R., Jenkin, M. E., Derwent, R. G., Hayman, G. D., Alfarra,
612 M. R., Coe, H., and McFiggans, G.: Simulating regional scale secondary organic
613 aerosol formation during the TORCH 2003 campaign in the southern UK, Atmos.
614 Chem. Phys., 6, 403-418, doi:10.5194/acp-6-403-2006, 2006.
615 Jordan, A., Haidacher, S., Hanel, G., Hartungen, E., Mark, L., Seehauser, H.,
616 Schottkowsky, R., Sulzer, P., and Mark, T. D.: A high resolution and high sensitivity
617 proton-transfer-reaction time-of-flight mass spectrometer (PTR-TOF-MS), Int. J.
618 Mass. Spectrom., 286, 122-128, 2009.
619 Kang, E., Toohey, D. W., and Brune, W. H.: Dependence of SOA oxidation on organic
620 aerosol mass concentration and OH exposure: experimental PAM chamber studies,
621 Atmos. Chem. Phys., 11, 1837-1852, doi:10.5194/acp-11-1837-2011, 2011.
622 Keywood, M. D., Varutbangkul, V., Bahreini, R., Flagan, R. C., and Seinfeld, J. H.:

623 Secondary Organic Aerosol Formation from the Ozonolysis of Cycloalkenes and
624 Related Compounds, Environ. Sci. Technol., 38, 4157-4164,
625 doi:10.1021/es035363o, 2004.
626 Kirchstetter, T. W., Harley, R. A., Kreisberg, N. M., Stolzenburg, M. R., and Hering, S.
627 V.: On-road measurement of fine particle and nitrogen oxide emissions from light-
628 and heavy-duty motor vehicles, Atmos. Environ., 33, 2955-2968,
629 doi:10.1016/S1352-2310(99)00089-8, 1999.
630 Kleindienst, T. E., Edney, E. O., Lewandowski, M., Offenberg, J. H., and Jaoui, M.:
631 Secondary Organic Carbon and Aerosol Yields from the Irradiations of Isoprene
632 and α-Pinene in the Presence of NO_x and SO_2, Environ. Sci. Technol., 40,
633 3807-3812, doi:10.1021/es052446r, 2006.
634 Kroll, J. H., Chan, A. W. H., Ng, N. L., Flagan, R. C., and Seinfeld, J. H.: Reactions
635 of Semivolatile Organics and Their Effects on Secondary Organic Aerosol
636 Formation, Environ. Sci. Technol., 41, 3545-3550, doi:10.1021/es062059x, 2007.
637 Kroll, J. H., Donahue, N. M., Jimenez, J. L., Kessler, S. H., Canagaratna, M. R.,
638 Wilson, K. R., Altieri, K. E., Mazzoleni, L. R., Wozniak, A. S., Bluhm, H., Mysak,
639 E. R., Smith, J. D., Kolb, C. E., and Worsnop, D. R.: Carbon oxidation state as a
640 metric for describing the chemistry of atmospheric organic aerosol, Nat. Chem., 3,
641 133-139, doi:10.1038/nchem.948, 2011.
642 Lelieveld, J., and Heintzenberg, J.: Sulfate Cooling Effect on Climate Through
643 In-Cloud Oxidation of Anthropogenic SO_2, Science, 258, 117-120,
644 doi:10.1126/science.258.5079.117, 1992.

645 Liggio, J., Li, S.-M., and McLaren, R.: Heterogeneous Reactions of Glyoxal on
646 Particulate Matter: Identification of Acetals and Sulfate Esters, Environ. Sci.
647 Technol., 39, 1532-1541, doi:10.1021/es048375y, 2005.
648 Lindinger, W., Hansel, A., and Jordan, A.: On-line monitoring of volatile organic
649 compounds at pptv levels by means of proton-transfer-reaction mass spectrometry
650 (PTR-MS) medical applications, food control and environmental research, Int. J.
651 Mass Spectrometry., 173, 191-241, doi:10.1016/S0168-1176(97)00281-4, 1998.
652 Liu, T. Y., Wang, X. M., Wang, B. G., Ding, X., Deng, W., Lü, S. J., and Zhang, Y. L.:
653 Emission factor of ammonia (NH_3) from on-road vehicles in China: tunnel tests in
654 urban Guangzhou, Environ. Res. Lett., 9, 064027,
655 doi:10.1088/1748-9326/9/6/064027, 2014.
656 Liu, T., Wang, X., Deng, W., Hu, Q., Ding, X., Zhang, Y., He, Q., Zhang, Z., Lü, S.,
657 Bi, X., Chen, J., and Yu, J.: Secondary organic aerosol formation from
658 photochemical aging of light-duty gasoline vehicle exhausts in a smog chamber,
659 Atmos. Chem. Phys., 15, 9049-9062, doi:10.5194/acp-15-9049-2015, 2015.
660 Loza, C. L., Chhabra, P. S., Yee, L. D., Craven, J. S., Flagan, R. C., and Seinfeld, J. H.:
661 Chemical aging of m-xylene secondary organic aerosol: laboratory chamber study,
662 Atmos. Chem. Phys., 12, 151-167, doi:10.5194/acp-12-151-2012, 2012.
663 Matsunaga, A., and Ziemann, P. J.: Gas-Wall Partitioning of Organic Compounds in a
664 Teflon Film Chamber and Potential Effects on Reaction Product and Aerosol Yield
665 Measurements, Aerosol Sci. Tech., 44, 881-892,
666 doi:10.1080/02786826.2010.501044, 2010.

667 Mauldin Iii, R. L., Berndt, T., Sipila, M., Paasonen, P., Petaja, T., Kim, S., Kurten, T.,
668 Stratmann, F., Kerminen, V. M., and Kulmala, M.: A new atmospherically relevant
669 oxidant of sulphur dioxide, Nature, 488, 193-196, doi:10.1038/nature11278, 2012.
670 McMurry, P. H., and Grosjean, D.: Gas and aerosol wall losses in Teflon film smog
671 chambers, Environ. Sci. Technol., 19, 1176-1182, doi:10.1021/es00142a006, 1985.
672 Nel, A.: Air Pollution-Related Illness: Effects of Particles, Science, 308, 804-806,
673 doi:10.1126/science.1108752, 2005.
674 Newland, M. J., Rickard, A. R., Alam, M. S., Vereecken, L., Munoz, A., Rodenas, M.,
675 and Bloss, W. J.: Kinetics of stabilised Criegee intermediates derived from alkene
676 ozonolysis: reactions with SO_2, H_2O and decomposition under boundary layer
677 conditions, Phys. Chem. Chem. Phys., 17, 4076-4088, doi:10.1039/C4CP04186K,
678 2015.
679 Ng, N. L., Kroll, J. H., Chan, A. W. H., Chhabra, P. S., Flagan, R. C., and Seinfeld, J.
680 H.: Secondary organic aerosol formation from m-xylene, toluene, and benzene,
681 Atmos. Chem. Phys., 7, 3909-3922, doi:10.5194/acp-7-3909-2007, 2007.
682 Ng, N. L., Canagaratna, M. R., Jimenez, J. L., Chhabra, P. S., Seinfeld, J. H., and
683 Worsnop, D. R.: Changes in organic aerosol composition with aging inferred from
684 aerosol mass spectra, Atmos. Chem. Phys., 11, 6465-6474,
685 doi:10.5194/acp-11-6465-2011, 2011.
686 Nordin, E. Z., Eriksson, A. C., Roldin, P., Nilsson, P. T., Carlsson, J. E., Kajos, M. K.,
687 Hellén, H., Wittbom, C., Rissler, J., Löndahl, J., Swietlicki, E., Svenningsson, B.,
688 Bohgard, M., Kulmala, M., Hallquist, M., and Pagels, J. H.: Secondary organic

689 aerosol formation from idling gasoline passenger vehicle emissions investigated in
690 a smog chamber, Atmos. Chem. Phys., 13, 6101-6116,
691 doi:10.5194/acp-13-6101-2013, 2013.
692 Ouyang, B., McLeod, M. W., Jones, R. L., and Bloss, W. J.: NO_3 radical production
693 from the reaction between the Criegee intermediate CH_2OO and NO_2, Phys. Chem.
694 Chem. Phys., 15, 17070-17075, doi:10.1039/C3CP53024H, 2013.
695 Parrish, D. D., and Zhu, T.: Clean Air for Megacities, Science, 326, 674-675,
696 doi:10.1126/science.1176064, 2009.
697 Pathak, R. K., Stanier, C. O., Donahue, N. M., and Pandis, S. N.: Ozonolysis of
698 alpha-pinene at atmospherically relevant concentrations: Temperature dependence
699 of aerosol mass fractions (yields), J. Geophys. Res.-Atmos, 112, D03201,
700 doi:10.1029/2006jd007436, 2007.
701 Pathak, R. K., Wu, W. S., and Wang, T.: Summertime $PM_{2.5}$ ionic species in four
702 major cities of China: nitrate formation in an ammonia-deficient atmosphere,
703 Atmos. Chem. Phys., 9, 1711-1722, doi:10.5194/acp-9-1711-2009, 2009.
704 Platt, S. M., El Haddad, I., Zardini, A. A., Clairotte, M., Astorga, C., Wolf, R., Slowik,
705 J. G., Temime-Roussel, B., Marchand, N., Ježek, I., Drinovec, L., Močnik, G.,
706 Möhler, O., Richter, R., Barmet, P., Bianchi, F., Baltensperger, U., and Prévôt, A. S.
707 H.: Secondary organic aerosol formation from gasoline vehicle emissions in a new
708 mobile environmental reaction chamber, Atmos. Chem. Phys., 13, 9141-9158,
709 doi:10.5194/acp-13-9141-2013, 2013.
710 Presto, A. A., Gordon, T. D., and Robinson, A. L.: Primary to secondary organic

711 aerosol: evolution of organic emissions from mobile combustion sources, Atmos.
712 Chem. Phys., 14, 5015-5036, doi:10.5194/acp-14-5015-2014, 2014.
713 Sato, K., Takami, A., Isozaki, T., Hikida, T., Shimono, A., and Imamura, T.: Mass
714 spectrometric study of secondary organic aerosol formed from the photo-oxidation
715 of aromatic hydrocarbons, Atmos. Environ., 44, 1080-1087,
716 doi:10.1016/j.atmosenv.2009.12.013, 2010.
717 Seinfeld, J. and Pandis, S. N.: From air pollution to climate change, Atmospheric
718 Chemistry and Physics, 2nd Edn., p. 208, 1998.
719 Shilling, J. E., Chen, Q., King, S. M., Rosenoern, T., Kroll, J. H., Worsnop, D. R.,
720 DeCarlo, P. F., Aiken, A. C., Sueper, D., Jimenez, J. L., and Martin, S. T.:
721 Loading-dependent elemental composition of α-pinene SOA particles, Atmos.
722 Chem. Phys., 9, 771-782, doi:10.5194/acp-9-771-2009, 2009.
723 Shindell, D. T., Faluvegi, G., Koch, D. M., Schmidt, G. A., Unger, N., and Bauer, S.
724 E.: Improved Attribution of Climate Forcing to Emissions, Science, 326, 716-718,
725 doi:10.1126/science.1174760, 2009.
726 Sipila, M., Berndt, T., Petaja, T., Brus, D., Vanhanen, J., Stratmann, F., Patokoski, J.,
727 Mauldin, R. L., Hyvarinen, A. P., Lihavainen, H., and Kulmala, M.: The Role of
728 Sulfuric Acid in Atmospheric Nucleation, Science, 327, 1243-1246,
729 doi:10.1126/science.1180315, 2010.
730 Taatjes, C. A., Welz, O., Eskola, A. J., Savee, J. D., Scheer, A. M., Shallcross, D. E.,
731 Rotavera, B., Lee, E. P. F., Dyke, J. M., Mok, D. K. W., Osborn, D. L., and Percival,
732 C. J.: Direct Measurements of Conformer-Dependent Reactivity of the Criegee

733 Intermediate CH_3CHOO, Science, 340, 177-180, doi:10.1126/science.1234689,
734 2013.
735 Volkamer, R., Jimenez, J. L., San Martini, F., Dzepina, K., Zhang, Q., Salcedo, D.,
736 Molina, L. T., Worsnop, D. R., and Molina, M. J.: Secondary organic aerosol
737 formation from anthropogenic air pollution: Rapid and higher than expected,
738 Geophys. Res. Lett., 33, L17811, doi:10.1029/2006gl026899, 2006.
739 Wang, X., and Wu, T.: Release of Isoprene and Monoterpenes during the Aerobic
740 Decomposition of Orange Wastes from Laboratory Incubation Experiments,
741 Environ. Sci. Technol., 42, 3265-3270, doi:10.1021/es702999j, 2008.
742 Wang, X., Liu, T., Bernard, F., Ding, X., Wen, S., Zhang, Y., Zhang, Z., He, Q., Lü, S.,
743 Chen, J., Saunders, S., and Yu, J.: Design and characterization of a smog chamber
744 for studying gas-phase chemical mechanisms and aerosol formation, Atmos. Meas.
745 Tech., 7, 301-313, doi:10.5194/amt-7-301-2014, 2014.
746 Welz, O., Savee, J. D., Osborn, D. L., Vasu, S. S., Percival, C. J., Shallcross, D. E.,
747 and Taatjes, C. A.: Direct Kinetic Measurements of Criegee Intermediate (CH_2OO)
748 Formed by Reaction of CH_2I with O_2, Science, 335, 204-207,
749 doi:10.1126/science.1213229, 2012.
750 Wexler, A. S. and Clegg, S. L.: Atmospheric aerosol models for systems including the
751 ions H^+, NH_4^+, Na^+, SO_4^{2-}, NO_3^-, Cl^-, Br^-, and H_2O, J. Geophys. Res., 107(D14),
752 4207, doi:10.1029/2001JD000451, 2002.
753 Xiao, R., Takegawa, N., Kondo, Y., Miyazaki, Y., Miyakawa, T., Hu, M., Shao, M.,
754 Zeng, L. M., Hofzumahaus, A., Holland, F., Lu, K., Sugimoto, N., Zhao, Y., and

Zhang, Y. H.: Formation of submicron sulfate and organic aerosols in the outflow from the urban region of the Pearl River Delta in China, Atmos. Environ., 43, 3754-3763, doi:10.1016/j.atmosenv.2009.04.028, 2009.

Yi, Z., Wang, X., Sheng, G., Zhang, D., Zhou, G., and Fu, J.: Soil uptake of carbonyl sulfide in subtropical forests with different successional stages in south China, J. Geophy. Res.-Atmos., 112, D08302, doi:10.1029/2006JD008048, 2007.

Zhang, Q., Jimenez, J. L., Canagaratna, M. R., Allan, J. D., Coe, H., Ulbrich, I., Alfarra, M. R., Takami, A., Middlebrook, A. M., Sun, Y. L., Dzepina, K., Dunlea, E., Docherty, K., DeCarlo, P. F., Salcedo, D., Onasch, T., Jayne, J. T., Miyoshi, T., Shimono, A., Hatakeyama, S., Takegawa, N., Kondo, Y., Schneider, J., Drewnick, F., Borrmann, S., Weimer, S., Demerjian, K., Williams, P., Bower, K., Bahreini, R., Cottrell, L., Griffin, R. J., Rautiainen, J., Sun, J. Y., Zhang, Y. M., and Worsnop, D. R.: Ubiquity and dominance of oxygenated species in organic aerosols in anthropogenically-influenced Northern Hemisphere midlatitudes, Geophys. Res. Lett., 34, L13801, doi:10.1029/2007gl029979, 2007.

Zhang, X., Cappa, C. D., Jathar, S. H., McVay, R. C., Ensberg, J. J., Kleeman, M. J., and Seinfeld, J. H.: Influence of vapor wall loss in laboratory chambers on yields of secondary organic aerosol, P. Natl. Acad. Sci., 111, 5802–5807, doi:10.1073/pnas.1404727111, 2014.

Zhang, X., Schwantes, R. H., McVay, R. C., Lignell, H., Coggon, M. M., Flagan, R. C., and Seinfeld, J. H.: Vapor wall deposition in Teflon chambers, Atmos. Chem. Phys., 15, 4197-4214, doi:10.5194/acp-15-4197-2015, 2015.

Zhang, Y., Guo, H., Wang, X., Simpson, I. J., Barletta, B., Blake, D. R., Meinardi, S., Rowland, F. S., Cheng, H., Saunders, S. M., and Lam, S. H. M.: Emission patterns and spatiotemporal variations of halocarbons in the Pearl River Delta region, southern China, J. Geophy. Res.-Atmos., 115, D15309, doi:10.1029/2009JD013726, 2010.

Zhang, Y., Wang, X., Blake, D. R., Li, L., Zhang, Z., Wang, S., Guo, H., Lee, F. S. C., Gao, B., Chan, L., Wu, D., and Rowland, F. S.: Aromatic hydrocarbons as ozone precursors before and after outbreak of the 2008 financial crisis in the Pearl River Delta region, south China, J. Geophy. Res.-Atmos., 117, D15306, doi:10.1029/2011JD017356, 2012.

Zhang, Y., Wang, X., Zhang, Z., Lü, S., Shao, M., Lee, F. S. C., and Yu, J.: Species profiles and normalized reactivity of volatile organic compounds from gasoline evaporation in China, Atmos. Environ., 79, 110-118, doi:10.1016/j.atmosenv.2013.06.029, 2013.

Zhang, Y., Wang, X., Zhang, Z., Lü, S., Huang, Z., and Li, L.: Sources of C2–C4 alkenes, the most important ozone nonmethane hydrocarbon precursors in the Pearl River Delta region, Sci. Total Environ., 502, 236-245, doi:10.1016/j.scitotenv.2014.09.024, 2015.

Zhang, Y. M., Zhang, X. Y., Sun, J. Y., Lin, W. L., Gong, S. L., Shen, X. J., and Yang, S.: Characterization of new particle and secondary aerosol formation during summertime in Beijing, China, Tellus B, 63, doi:10.3402/tellusb.v63i3.16221, 2011.

799 **Table 1.** Detailed information of the three LDGVs.

ID	Emission standard class	Vehicle	Model year	Mileage (km)	Displacement (cm^3)	Power (kW)	Weight (kg)
Ⅰ	Euro4	Golf	2011	25000	1598	77	1295
Ⅱ	Euro4	Sunny	2011	9448	1498	82	1069
Ⅲ	Euro1	Accord	2002	237984	2298	110	1423

800

801

802

803 **Table 2.** Summary of the initial conditions during the photooxidation of LDGV
804 exhaust.

Exp #[a]	OH ($\times10^6$ molecules cm^{-3})	T (℃)	RH (%)	VOC /NO_x	NMHCs (ppbv)	NO (ppbv)	NO_2 (ppbv)	SO_2 (ppbv)
I–1	0.88	25.0±0.8	52.9±2.0	9.3	2896	300.6	9.5	8.6
I–2	1.19	25.5±0.3	53.6±2.5	7.7	2323	281.4	19.5	151.8
I–3[b]	1.45	23.9±0.9	59.0±4.1	7.9	2447	300.0	10.2	8.9
II–1	1.29	24.6±0.5	52.5±1.7	10.8	4313	374	24.7	9
II–2	1.08	24.2±0.7	55.9±2.5	9	3220	356	2.6	151.9
III–1	0.73	24.1±0.6	57.0±2.0	6	2582	431	0.6	9.2
III–2	0.79	24.3±0.3	57.9±1.2	4.9	2243	454.6	3.9	154.1

805 [a] Photooxidation experiments of LDGV exhaust named with I, II and III refers to different
806 vehicles.
807 [b] Ammonium sulfate (53.3 μg m^{-3}) was introduced as seed aerosols.
808

809 **Table 3.** Summary of the final results during the photooxidation of LDGV exhaust.

Exp #	POA ($\mu g\ m^{-3}$)	SOA ($\mu g\ m^{-3}$)	Sulfate ($\mu g\ m^{-3}$)	Ammonium ($\mu g\ m^{-3}$)	Nitrate ($\mu g\ m^{-3}$)	Particle number (cm^{-3})[a]	$[H^+]$[b] ($nmol\ m^{-3}$)
I–1	0.31	77.6	0.7	17.1	65.9	85182	12.5
I–2	0.21	91.2	67.5	17.6	6.1	563705	21.9
II–1	0.28	30.7	-	2.6	5.6	7427	10.4
II–2	0.13	37.3	38.1	9.7	1.9	357673	16.5
III–1	0.17	17.6	-	0.1	0.7	116143	7.4
III–2	0.23	77	76.7	19.2	5.3	630620	27.1

810 [a] Maximum particle number concentrations were without wall loss corrections.

811 [b] The concentration of H^+ in particle phase shown here was the value when the SOA formation rate

812 reached the maximum during each experiment.

813

814 **Table 4.** Concentrations of alkenes included in the model and the category of sCIs.

Sepecies	Concentration (ppb)			sCIs
	I-2	II-2	III-2	
ethene	333.1	113.8	202.0	CH_2OO
propene	95.8	50.3	52.6	CH_2OO, CH_3CHOO
1-butene	30.9	49.1	13.1	CH_2OO, C_2H_5CHOO
cis-2-butene	7.6	4.8	7.1	CH_3CHOO
trans-2-butene	9.9	6.4	9.6	CH_3CHOO
1-pentene	3.8	0.3	3.1	CH_2OO, C_3H_7CHOO
cis-2-pentene	5.2	1.2	5.2	CH_3CHOO, C_2H_5CHOO
trans-2-pentene	8.5	2.6	9.4	CH_3CHOO, C_2H_5CHOO
2-methyl-1-butene	11.9	5.4	12.4	CH_2OO, $C_2H_5(CH_3)COO$
3-methyl-1-butene	2.4	0.8	2.4	CH_2OO, $(CH_3)_2CHCHOO$
2-methyl-2-butene	17.8	10.9	22.7	CH_3CHOO, $(CH_3)_2COO$
cis-2-hexene	0.8	0	1.5	CH_3CHOO, C_3H_7CHOO

815

816

817 **Table 5.** Summary of the final results during the photooxidation of LDGV exhaust.

Stabilized CIs	10^{15} K_{R2} (cm^3 $molecule^{-1}s^{-1}$)	10^{11} K_{R3} (cm^3 $molecule^{-1}s^{-1}$)	10^{12} K_{R4} (cm^3 $molecule^{-1}s^{-1}$)	K_{R5} (s^{-1})
CH_2OO	0.025[a]	3.9[b]	7.0[b]	0[c]
CH_3CHOO	7.0[d]	4.55[d]	2.0[d]	67.5[e]
$(CH_3)_2COO$	2.1[c]	2.4[c]	2.0[c]	151[c]

818 [a] (Ouyang et al., 2013); [b] (Welz et al., 2012); [c] (Newland et al., 2015); [d] (Taatjes et al., 2013);

819 [e] Average of K_{R5} from Fenske et al. (2000) and Newland et al. (2015).

820

821 **Table 6.** Partitioning coefficients for different C_i^* calculated using gas-particle
822 partitioning theory.

$\log_{10} C_i^*$ ($\mu g\ m^{-3}$)	I-1	I-2	II-1	II-2	III-1	III-3
-2	1.000	1.000	1.000	1.000	0.999	1.000
-1	0.999	0.999	0.997	0.997	0.994	0.999
0	0.987	0.989	0.968	0.974	0.946	0.987
1	0.886	0.901	0.754	0.789	0.638	0.885
2	0.437	0.477	0.235	0.272	0.150	0.435
3	0.072	0.084	0.030	0.036	0.017	0.071
4	0.008	0.009	0.003	0.004	0.002	0.008
5	0.001	0.001	0.000	0.000	0.000	0.001
6	0.000	0.000	0.000	0.000	0.000	0.000

823
824

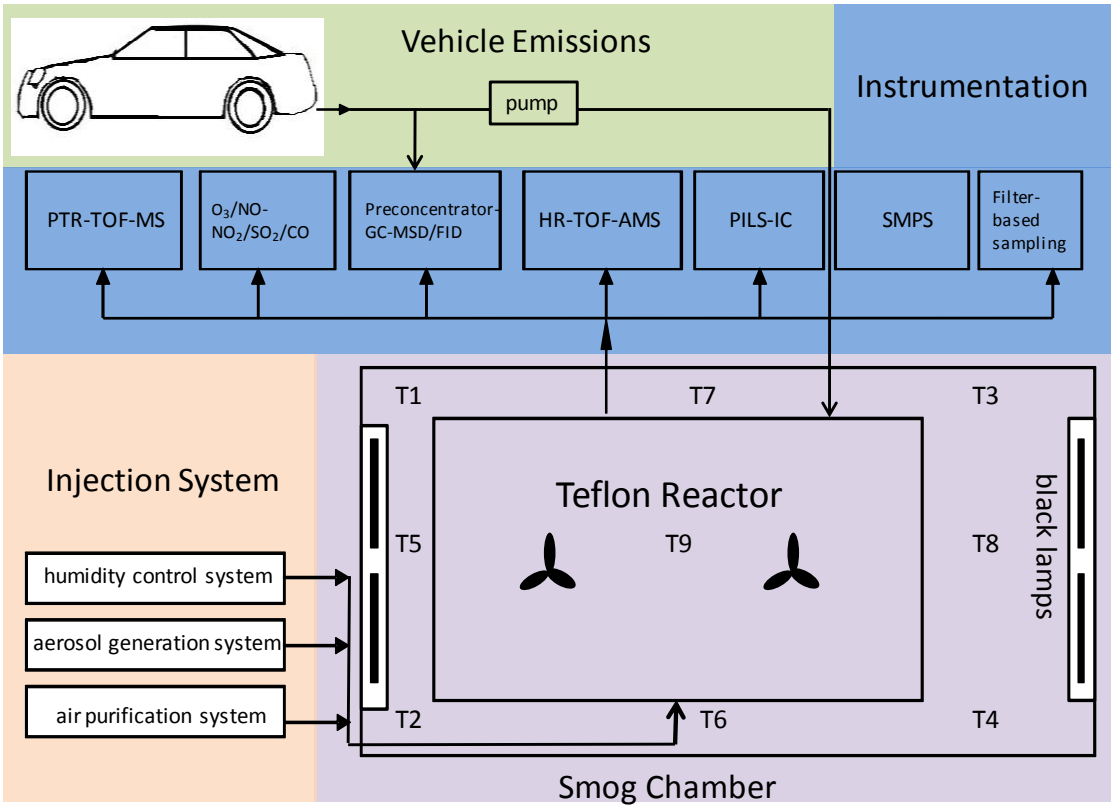

825

826 **Fig. 1.** Schematic of the GIG-CAS smog chamber facility and vehicle exhaust

827 injection system.

828

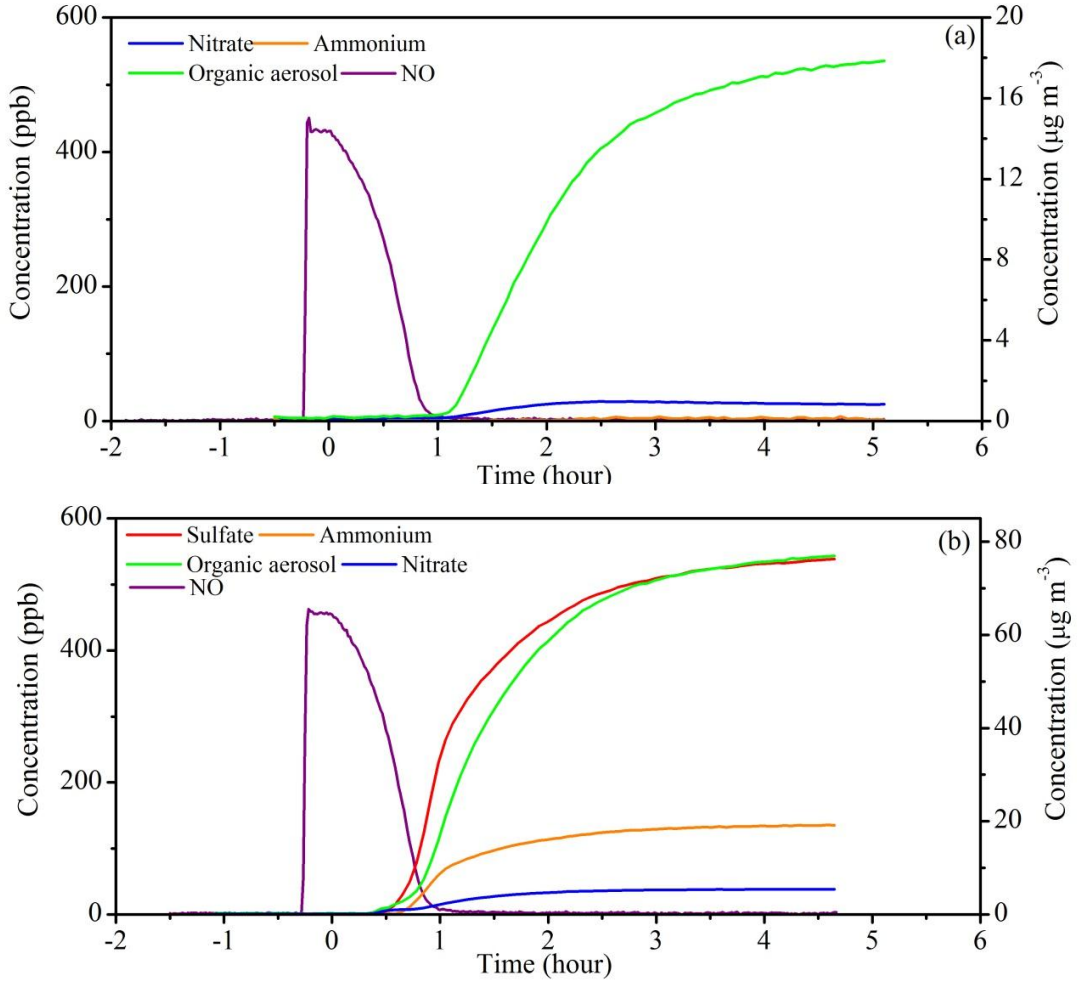

829

830 **Fig. 2.** Concentration–time plots of NO (left-y axis) and particle–phase species
831 (right-y axis) during the photochemical aging of emissions from vehicle III. (a)
832 Without SO_2, and (b) with SO_2. The concentrations of particle-phase species are
833 wall-loss corrected. At time =0 h, the black lamps were turned on.

834

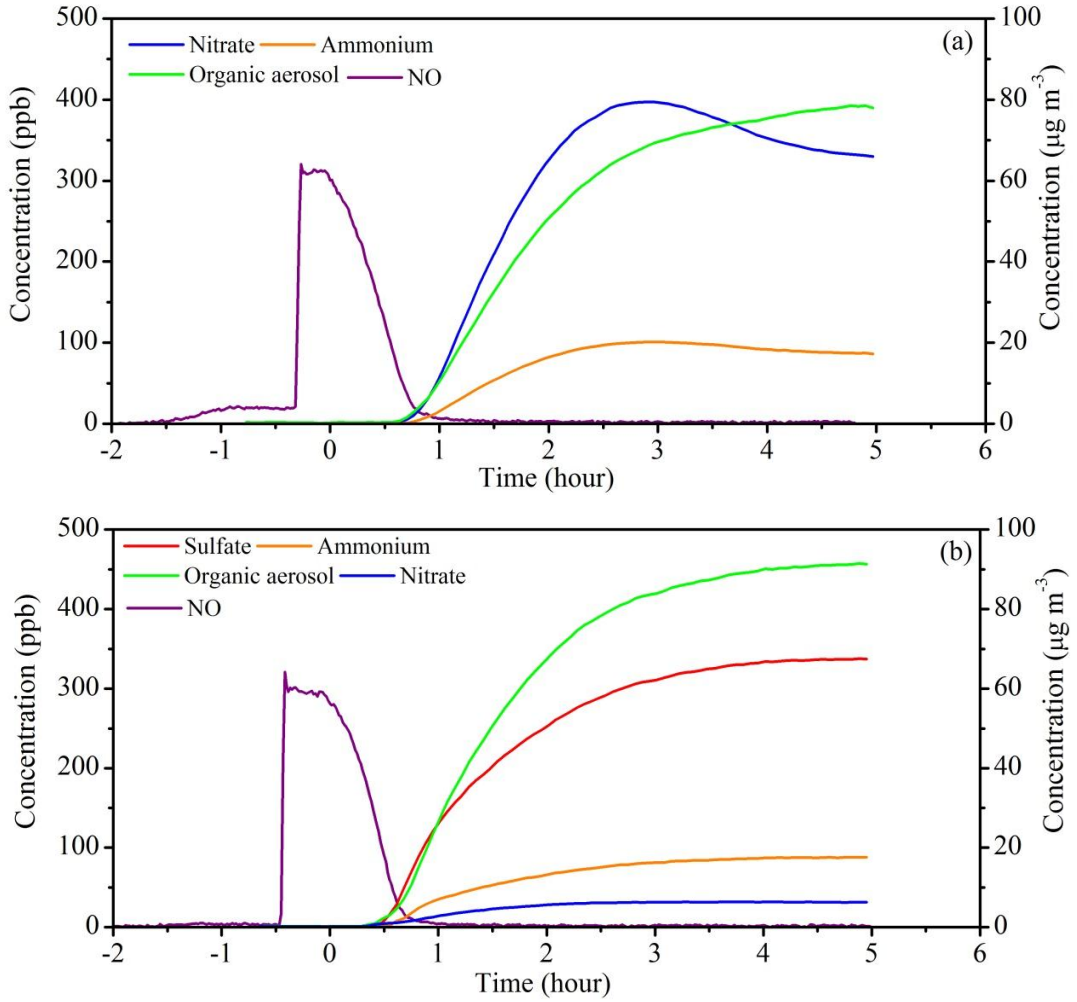

835

836 **Fig. 3.** Concentration–time plots of NO (left-y axis) and particle–phase species

837 (right-y axis) during the photochemical aging of emissions from vehicle I. (a) Without

838 SO_2, and (b) with SO_2. The concentrations of particle-phase species are wall-loss

839 corrected. At time =0 h, the black lamps were turned on.

840

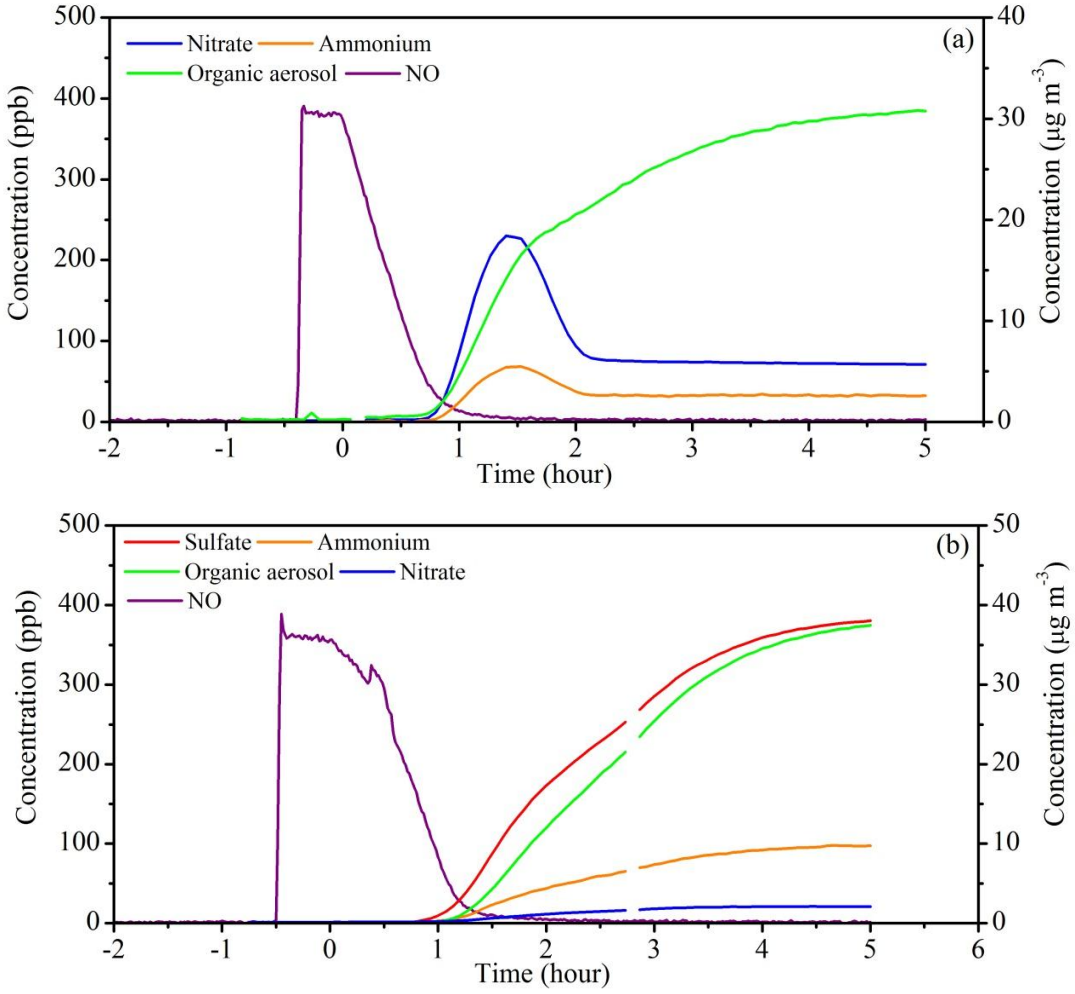

841

842 **Fig. 4**. Concentration–time plots of NO (left-y axis) and particle–phase species
843 (right-y axis) during the photochemical aging of emissions from vehicle II. (a)
844 Without SO_2, and (b) with SO_2. The concentrations of particle-phase species are
845 wall-loss corrected. At time =0 h, the black lamps were turned on.

846

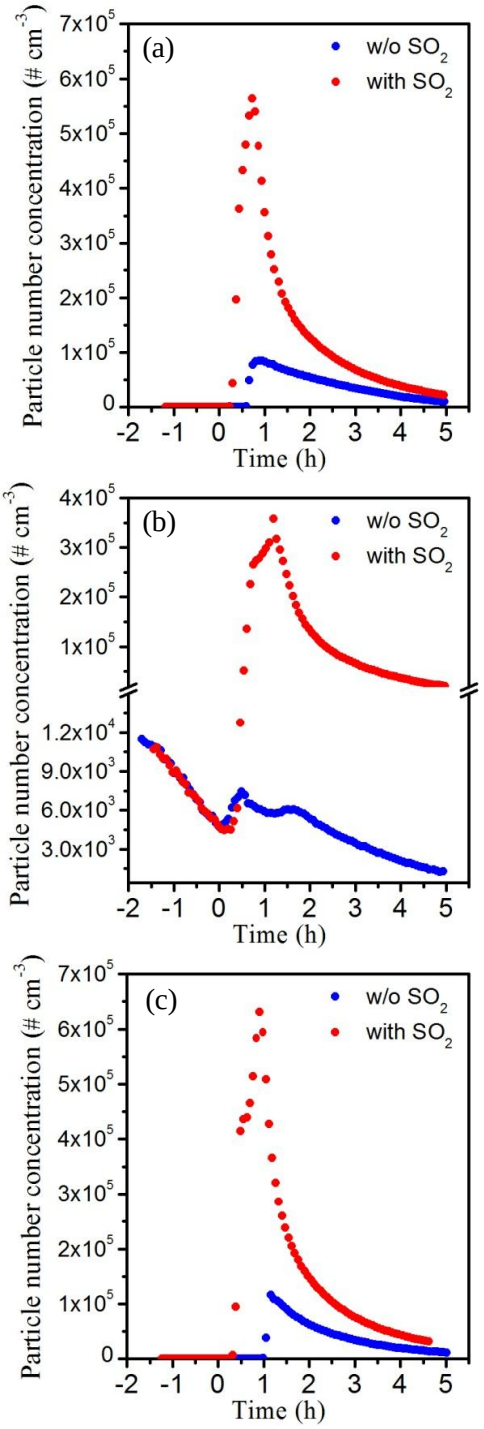

847

848 **Fig. 5**. Evolution of particle number concentrations during the aging experiments of

849 LDGV exhaust for vehicle I (a), II (b) and III (c). At time =0 h, the black lamps were

850 turned on. W/o SO_2 and with SO_2 in the figures represent experiments without and

851 with adding SO_2, respectively.

852

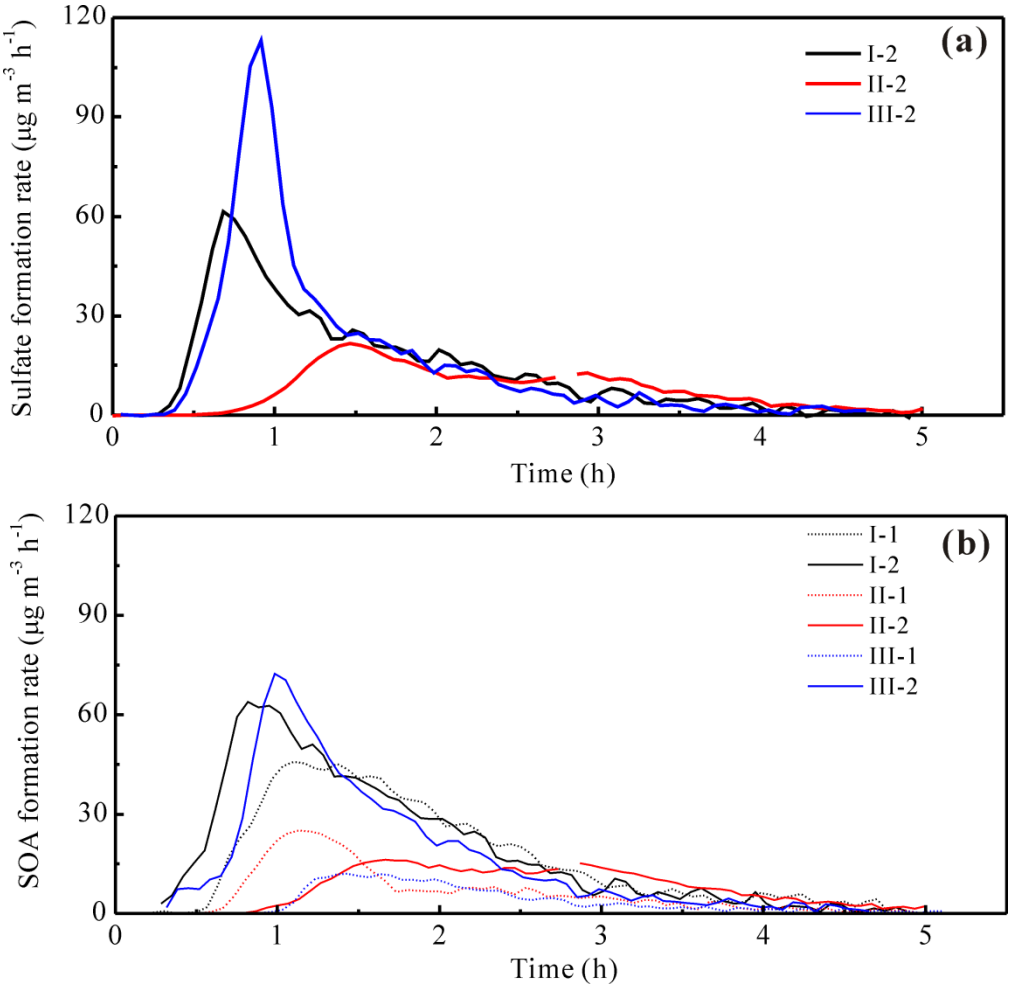

853

854 **Fig. 6.** Sulfate formation rates (**a**) and SOA formation rates (**b**) as a function of time

855 during the photooxidation of LDGV exhaust.

856

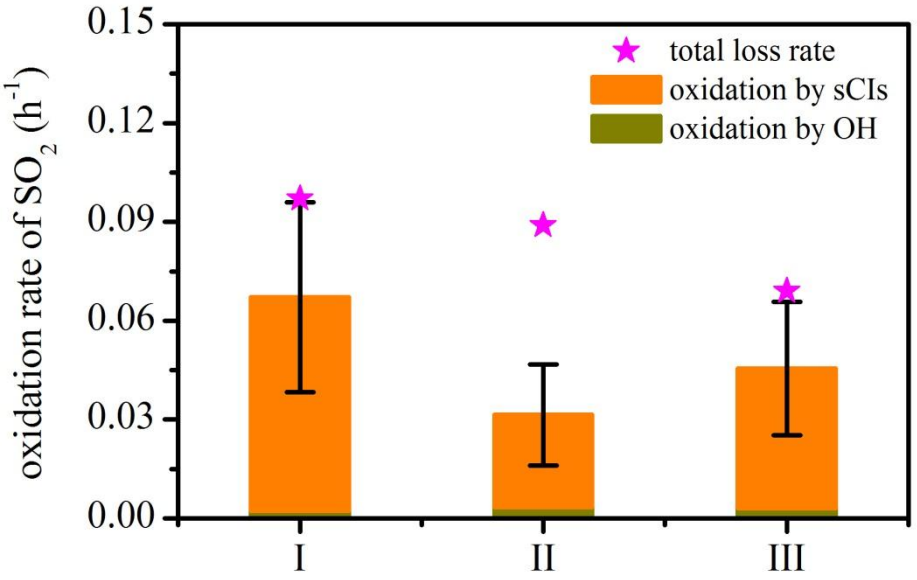

857

858 **Fig. 7.** The oxidation rate of SO_2 during the photooxidation of LDGV exhaust with
859 SO_2. The loss rates of SO_2 reacting with OH radicals and sCIs were calculated by
860 multiplying the reaction rate coefficients derived from the MCM v3.3 by the average
861 OH concentration and estimated sCIs concentration, respectively. Error bars represent
862 the standard derivation (1σ) of the oxidation rate of SO_2 by sCIs throughout the whole
863 experiment.

864
865

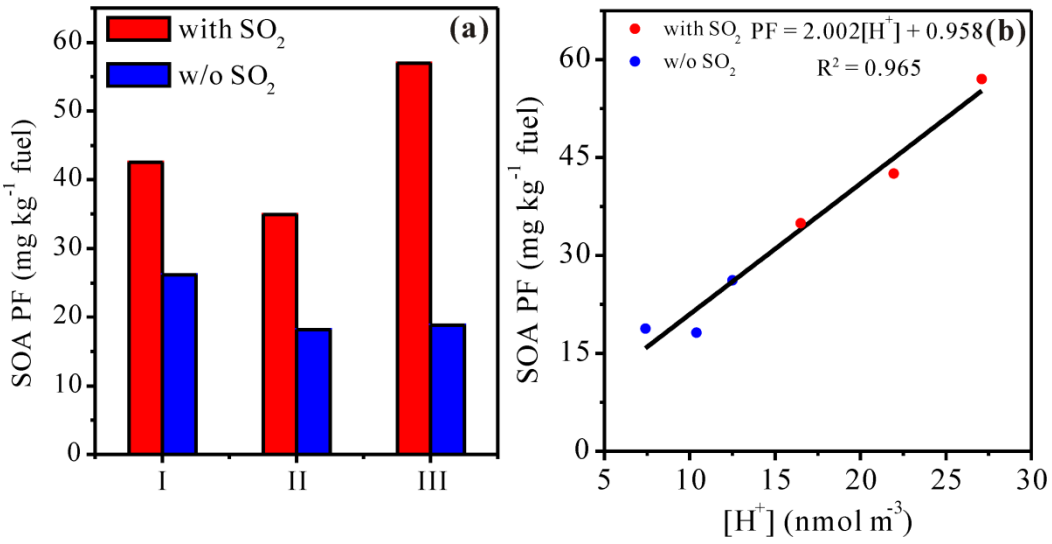

866

867 **Fig. 8**. SOA production factor (PF) and its relationship with particle acidity. (**a**) SOA

868 PF after 5 h of photochemical aging of exhaust from different LDGVs with and

869 without additional SO_2. (**b**) SOA PF as a function of in-situ particle acidity. The

870 concentration of H^+ in particle phase shown here was the value when the SOA

871 formation rate reached the maximum during each experiment.

872

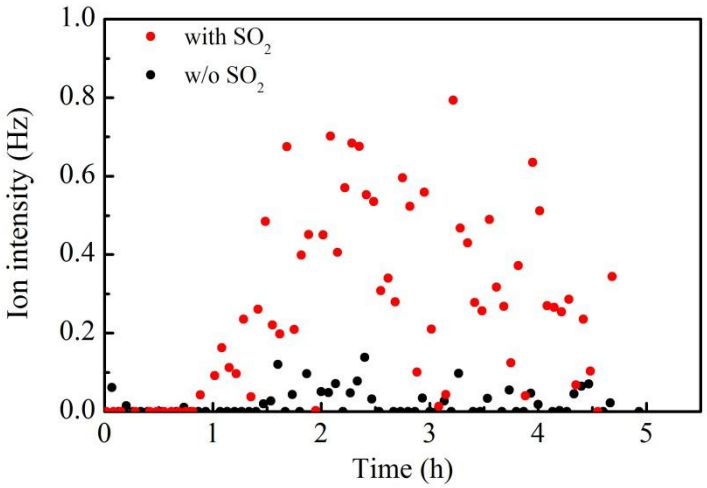

873

874 **Fig. 9**. Time evolution of m/z 88 during the aging of LDGV exhaust from vehicle III.

875

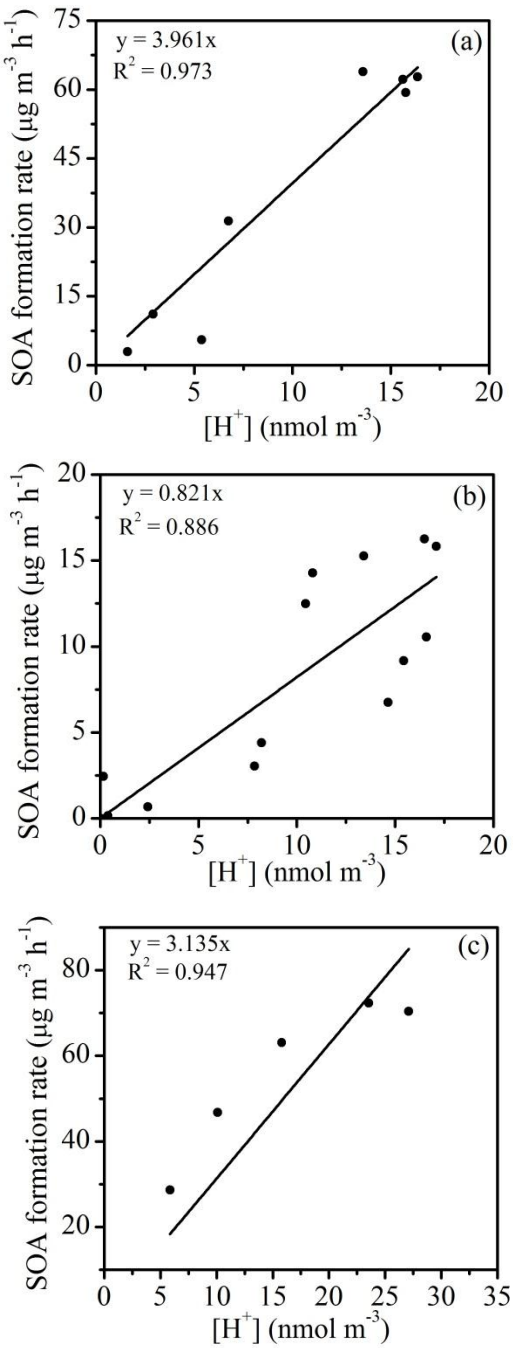

876

877 **Fig. 10.** SOA formation rate as a function of in-situ particle acidity ($[H^+]$) for vehicle

878 I (a), vehicle II (b) and vehicle III (c) with adding SO_2. Plotted data were selected

879 from when SOA formation rate was higher than zero to when the rate reached the

880 maximum value.

881

882

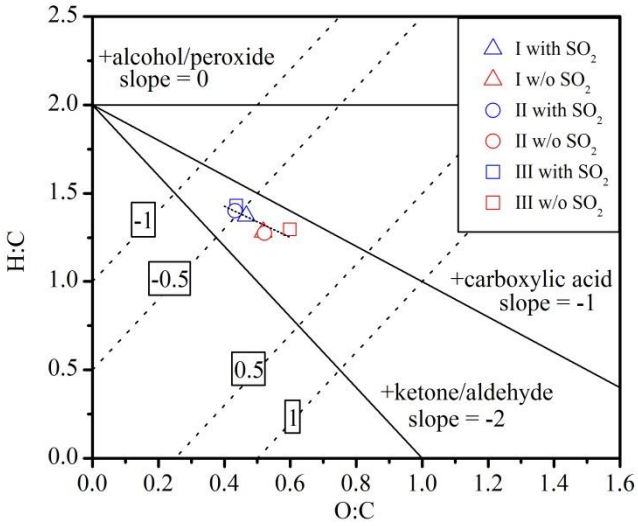

883

884 **Fig. 11.** O:C vs. H:C of SOA formed from LDGV exhaust with and without additional

885 SO_2 at the end of each experiment. Blue and red symbols represent data with and

886 without additional SO_2, respectively. The dashed lines represent estimated average

887 carbon oxidation states of -1, -0.5, 0.5 and 1 (Kroll et al., 2011). The black lines

888 represent the addition of functional groups to an aliphatic carbon (Heald et al., 2010).